

## Article

# Research on the Factors Affecting the Formation of Ore-Free Zone at Blast Furnace Throat Based on DEM

Hao Xu <sup>1</sup>, Yici Wang <sup>1,\*</sup>, Chuanhui Li <sup>2</sup>, Hongwei Guo <sup>3</sup> and Bingji Yan <sup>3,\*</sup>

<sup>1</sup> College of Materials and Metallurgy, Inner Mongolia University of Science and Technology, Baotou 014010, China; xu525167948@163.com

<sup>2</sup> Shandong Tianming Heavy Industry Technology Co., Ltd., Jinan 271100, China

<sup>3</sup> School of Iron and Steel, Soochow University, Suzhou 215131, China

\* Correspondence: wangyici01060@163.com (Y.W.); bjyan@suda.edu.cn (B.Y.)

**Abstract:** The ore-free zone in the center of the blast furnace throat is a major feature of the charging system, ensuring the permeability of the center. Factors that influence the formation of the ore-free zone need to be researched to increase the control precision. In this paper, on the basis of a 1:1 3D model of a blast furnace, the formation of an ore-free zone at the burden surface at the throat was simulated by using the discrete element method (DEM). The effects of burden line depth, batch weight, and distribution angle on the formation of ore-free zones were investigated. The results showed that with increasing burden line depth, the width of the ore-free zone increased, the thickness decreased, the ore-to-coke ratio decreased, and the central airflow developed. Only changing the ore batch weight affected the thickness and width of the ore-free zone and had a greater impact on the permeability of the ore-free zone. The greater the ore batch weight was, the worse the permeability, while changing the batch weight of both coke and ore mainly affected the thickness of the ore-free zone. The greater the batch weight of coke and ore was, the greater the thickness of the ore-free zone. In the case of changing only the angle of ore in the matrix, with the angle increasing, the ore-to-coke ratio around the ore-free zone decreased, the ore-to-coke ratio around the furnace wall increased, and the edge airflow was suppressed. In the case of changing the angle of coke and ore at the same time, with the simultaneous increase in both angles, the ore-free area was compressed in the direction of smaller charge segregation, the area with better permeability in the center of the furnace throat was reduced, and the central airflow was suppressed.

**Keywords:** blast furnace charging; DEM; ore-free zone; influencing factors; ore-to-coke ratio



**Citation:** Xu, H.; Wang, Y.; Li, C.; Guo, H.; Yan, B. Research on the Factors Affecting the Formation of Ore-Free Zone at Blast Furnace Throat Based on DEM. *Processes* **2023**, *11*, 967. <https://doi.org/10.3390/pr11030967>

Academic Editors: Shengchao Duan, Hanjie Guo, Jae Hong Shin, Yong Wang and Changyong Chen

Received: 8 February 2023

Revised: 13 March 2023

Accepted: 16 March 2023

Published: 22 March 2023



**Copyright:** © 2023 by the authors. Licensee MDPI, Basel, Switzerland. This article is an open access article distributed under the terms and conditions of the Creative Commons Attribution (CC BY) license (<https://creativecommons.org/licenses/by/4.0/>).

## 1. Introduction

In blast furnace production, a reasonable charging system is the key for the propitious operation, which not only plays a decisive role in the permeability of the burden but is also an important condition for the stable and smooth operation of the blast furnace [1,2]. Currently, there are two main charging forms for bell-less blast furnaces, namely, platform plus funnel and central coke charging. The burden surface under these two types has significant advantages, including stable charging shape and flexible adjustment [3,4]. The charging system of the platform plus funnel distributes the coke to the ore burden surface according to the gear. In this process, the large coke particles will roll down to the center of throat to improve the permeability at the center of the furnace throat. This charging system requires good rolling of coke particles, uniform particle size, and close to spherical shape [5]. The central coke is distributed to the center of the blast furnace through a rotating chute with a small inclination angle. Both of these two charging systems will form an ore-free zone in the center of the throat to a certain extent. The effect of central coke charging is most obvious, and the ore-free zone can effectively improve the permeability of the center of the blast furnace [6]. For the blast furnace using pulverized coal injection technology, when the quality of pulverized coal injection is increased, the central airflow will be strengthened,

and it is necessary to change the burden distribution to increase the permeability of the central area [7]. Therefore, the central charging system plays a vital role in the permeability of a blast furnace.

The formation of the ore-free area needs two steps. Firstly, coke charging is carried out at a small angle so that the middle zone and the central area of the burden surface are covered with coke; then, the ore is charged onto coke in the process of ore charging. It is very difficult to obtain direct information of the movement and distribution of the burden by physical means, so some researchers have provided theoretical guidance to blast furnace operators by developing mathematical models to predict the movement of particles within the blast furnace. M. Li et al. [8] obtained the trajectory of the burden, the shape of the burden profile, and the top ore-to-coke curve by calculating the charging process and produced software for predicting the burden profile, and the results correlated well with the actual data. Z. J. Teng et al. [9] developed a mathematical model with the Coriolis force and gas drag force to predict the trajectory of the burden, and comparing the velocity of particles at the end of the chute considering Coriolis forces with not considering them, they found that the former was 0.7 m/s smaller than the latter. G.L. Zhao et al. [10] established a mathematical model for the movement of the burden on rectangular and semicircular chutes, verified the correctness of the model with measured data, and studied the circumferential variation law of the burden on the chute. L.J. Wang et al. [11] considered the mass conservation, charging shape description, and falling point function, and the mathematical model description between the burden distribution matrix and the charging shape in the blast furnace charging process was studied. The model was tested based on the simulation experiment of the industrial process. In addition, some scholars have also established an off-line physical simulation model. T. Mitra et al. [12] scaled down the blast furnace equally and simulated the movement and distribution of the burden inside the furnace in the laboratory, focusing on the formation of coke and ore layers on the surface of the burden. H. Wei et al. [13] made a 1:10 equivalent scale model based on a blast furnace and conducted an experimental study on the radial porosity distribution of the coke layer, which showed that the porosity decreases with the increasing mass fraction of small particles. Both the mathematical model and the small-scale physical model, in which the obtained information on the burden motion and distribution is very limited, are not sufficiently comprehensive for the characterization of the charge motion in the complex conditions of the blast furnace.

In recent years, many researchers have used the discrete element method (DEM) to study blast furnace charging. Compared with mathematical models and experimental methods, the discrete element method can describe the movement of the charge in the throat more clearly, which is very effective for dealing with the problems of burden flow and squeezing. Liu et al. [14] investigated the effect of chute inclination, chute type, and burden line depth on the material flow trajectory using the discrete element method. H.Y. Ma et al. [15] studied the segregation of the burden distribution phenomenon under different chutes and found that the uniform burden distribution at the square outlet was conducive for accurate charging, and the uneven burden distribution in the broken chute increases the segregation of the burden distribution. H. Mio et al. [16] used the DEM model to study the radial burden distribution and average particle size distribution of the ore-coke mass ratio (O/C) of the burden surface. The simulation results are very close to the actual measurement results, which prove that it is feasible to use the discrete element method to simulate the burden distribution process of the bell-less blast furnace.

For blast furnaces, the airflow in the center of the furnace throat is developed due to the presence of the ore-free zone [17], but the excessive development of the airflow can lead to a significant decrease in gas utilization, and it is necessary to investigate the factors affecting the formation of the ore-free zone and the conditions affecting the extent of the ore-free zone to provide theoretical support for producers to adjust the charging system. Therefore, based on the discrete element method the discrete element software EDEM2021 is used for simulation. This paper establishes a 1:1 geometric model

of a 1750 m<sup>3</sup> bell-less blast furnace, which is running in a steel plant in Sichuan Province, and studies the influence of material line depth, batch weight, and distribution angle on the formation of ore-free zones.

## 2. Materials and Methods

### 2.1. Discrete Element Method

For particles with kinematic behavior, contact and collisions occur during motion, which in turn generate forces between the particles. To study the contact, collision, and motion between the particles of the burden in the blast furnace, simulations were performed using the discrete element method [18,19]. During the calculations, Newton's second law was used for the particles with contact. The normal collision force between the furnace particles causes the particles to produce translational motion, and the tangential contact force causes the particles to produce rotational motion. The equations for calculating the normal and tangential contact forces are shown in Equations (1) and (2) [20]:

$$F_{n,ij} = \left( K_n \Delta u_{n,ij} + \eta_n \frac{\Delta u_{n,ij}}{\Delta t} \right) \mathbf{n}_{ij} \quad (1)$$

$$F_{t,ij} = \min \left\{ \mu |F_{n,ij}| \mathbf{t}_{t,ij}, \left[ K_t (\Delta u_{t,ij} + \Delta \phi_{ij}) + \eta_t \left( \frac{\Delta u_{t,ij} + \Delta \phi_{ij}}{\Delta t} \right) \right] \mathbf{t}_{ij} \right\} \quad (2)$$

where  $K$  is the spring coefficient;  $\eta$  is the damping coefficient;  $\Delta u$  is the relative translational displacement of the gravitational center between two particles;  $\Delta \phi$  is the relative displacement of the contact point due to particle rotation;  $\mu$  is the frictional coefficient; and  $\mathbf{n}_{ij}$  and  $\mathbf{t}_{ij}$  denote the unit vector from the  $i$ -th particle to the  $j$ -th particle in the normal and tangential components, respectively. The subscripts  $n$  and  $t$  also denote the normal and tangential components, respectively. The translational and rotational motions of each particle are shown in Equations (3) and (4):

$$\dot{v} = \frac{\sum F}{m} + \mathbf{g} \quad (3)$$

$$\dot{\omega} = \frac{\sum M}{I} \quad (4)$$

where  $v$  is the vector of a particle velocity,  $F$  is the contact force acting on a particle,  $m$  and  $\mathbf{g}$  are the mass of a particle and the gravitational acceleration,  $\omega$  is the vector of angular velocity, and  $M$  and  $I$  denote the moment caused by the tangential force and the moment of inertia.

### 2.2. Parameters Used in Simulation Process

When using the discrete element method for simulation, the parameters are important factors affecting the final simulation results, which mainly include material properties and inter-material contact parameters. In order to improve the computational efficiency, it is assumed that the burden particles are all spherical. All the particle sizes as follows refer to the diameter of the real particles in production. Tables 1–3 are the main particle size distribution used in the 1750 m<sup>3</sup> blast furnace. Based on these data, the Ore1 particles in the charging are set as the following particle size percentages: 20 mm (30%), 34 mm (40%), 64 mm (20%), 90 mm (10%); the corresponding ore particles in the base burden surface (ore bed) are set as Ore2 with a particle size of 50 mm (100%), with no contact between Ore1 and Ore2 in the simulation phase. The coke particles in the five charging gears of 38.5°, 36.5°, 34.5°, 32.5°, and 30.5° are Coke1, the coke particles in the center gear of 22.5° are Coke2, and the particle size of both Coke1 and Coke2 is 50 mm.

**Table 1.** The particle size proportion of sinter.

Particle Size (mm)	Percentage (%)
>40	4
40~25	17
25~10	57
10~5	20
<5	2

**Table 2.** The particle size proportion of pellets.

Particle Size (mm)	Percentage (%)
>20	0.8
20~10	98.8
<10	0.4

**Table 3.** The particle size proportion of coke.

Particle Size (mm)	Percentage (%)
>80	2
80~60	24.2
60~40	42
40~25	27.8
<25	4

### 2.2.1. Material Properties

The material properties of different raw materials in the simulation process include Poisson's ratio, density, and shear modulus, and the above three parameters have been taken closer in many simulations in the past. The material properties used in this paper are shown in Table 4.

**Table 4.** Material properties of blast furnace materials.

Parameters	Symbols	Coke	Ore	Steel	Unit
Poisson's ratio	$\nu$	0.22	0.25	0.25	-
Density	$\rho$	1000	3200	7850	$\text{kg}\cdot\text{m}^{-3}$
Shear modulus	$G$	$1 \times 10^8$	$1 \times 10^8$	$1 \times 10^8$	Pa

### 2.2.2. Contact Parameters between Materials

The contact parameters used in the discrete element method simulation include the restitution coefficient, rolling coefficient, and static coefficient. These parameters will affect the heap angle, platform width, and depth of the burden surface shape. In the simulation of blast furnace burden distribution, there are contact relationships between the burden and the burden and between the burden and the metal chute. This paper refers to the simulation parameters used by many scholars in the past [18,19,21–23] and summarizes the parameter range, as shown in Table 5.

**Table 5.** The value range of relationship parameters between the contact systems in the charging system.

Interaction	Restitution Coefficient	Static Friction	Rolling Friction
Coke and coke	0.15–0.45	0.1–0.25	0.1–0.2
Coke and ore	0.2–0.35	0.2–0.5	0.05–0.3
Ore and ore	0.3–0.6	0.2–0.5	0.02–0.15
Coke and chute	0.3–0.5	0.3–0.6	0.1–0.2
Ore and chute	0.3–0.5	0.3–0.6	0.05–0.1

Figure 1 shows the shape of the coke and ore burden surfaces in the 1750 m<sup>3</sup> BF. The width of the left platform is 1.01 m, the width of the right platform is 1.13 m, the outer pile angle of the left half of the burden surface is 5°, the outer pile angle of the right half of the burden surface is 6°, and the depth of the burden surface is 0.78 m. Since the center of the furnace throat forms an ore-free area after laying ore, the inner pile angle of the ore burden surface is not considered.

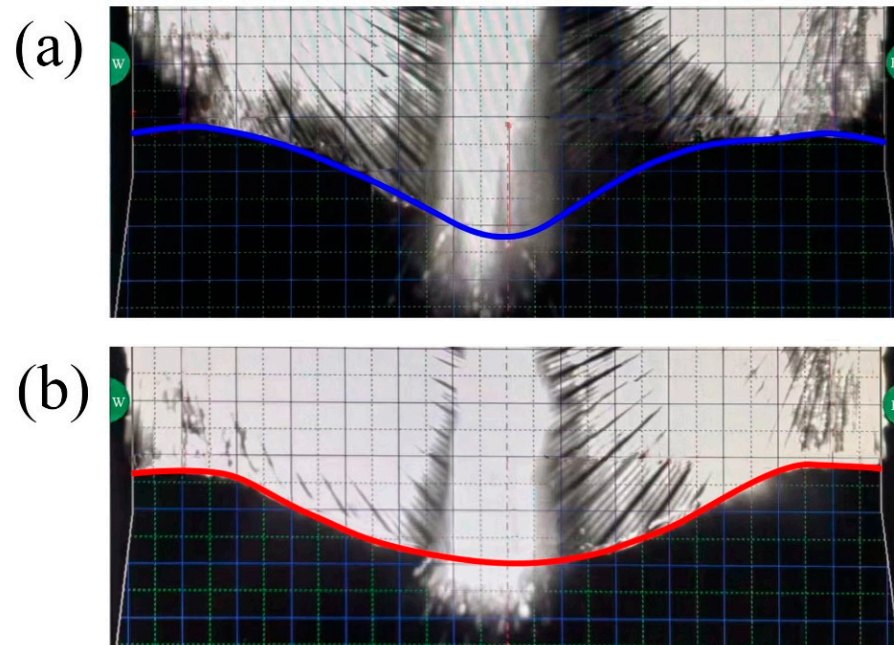


**Figure 1.** Blast furnace burden surface measured diagram: (a) coke burden surface shape; (b) ore burden surface shape.

After obtaining the data for the actual burden surface, the restitution coefficient and friction factor used for the simulation are discussed. In general, the restoration coefficient of an object is the ratio of the velocity of the object when it is about to touch another object to the velocity of the object leaving after contact. After several simulations, it can be concluded that the restoration coefficient between the charges affects the dispersion of the charge after it falls to the burden surface; the higher the restitution coefficient is, the greater the dispersion. When there is no liner in the chute, the higher the restoration coefficient between the charge and the chute, the greater the dispersion of the charge falling on the chute; when there is a liner in the chute, some ore and coke particles will accumulate between the liner, and after the charge falls from the center throat plate, most of the charge will be in contact with the particles between the liner, not with the chute, so the restoration coefficient between the charge and the chute has less influence on the degree of dispersion.

In the charging simulation process, friction exists between different burden particles as well as between the burden and the metal chute. The friction between the charges mainly affects the rolling of the charge on the burden surface; the higher the friction is, the higher the natural accumulation angle of the charge will be. The friction between the charge and the metal chute mainly affects the velocity of the charge after it leaves the chute, which determines the position of the charge's landing point on the burden surface and thus affects the shape of the burden surface. Figure 2 shows the actual measurement at the furnace throat, from which it can be found that the airflow is strong at the center of the furnace throat, accompanied by the phenomenon that the charge is blown up (the circled part in the picture is the blown burden), so the rollability of the laid coke in the center of the furnace throat at a small angle will be greatly affected. To reflect the effect of airflow in the discrete element simulation, the approach taken is to equate the effect of airflow to the increase in friction factor, that is, to increase the rolling friction and static friction between

Coke2 and other particles during the simulation, and the specific contact parameters are introduced in Section 2.3.



**Figure 2.** Phenomenon of the charge being blown up by the gas flow at the center of the furnace throat.

### 2.3. Model of Burden Distribution and Parameters

This paper takes 1750 m<sup>3</sup> BF equipment of a steel plant as a prototype. The blast furnace uses the technology of pulverized coal injection to replace part of the coke, with the injection velocity of 34 t pulverized coal per hour on average, and the coal ratio (the amount of pulverized coal consumed by the blast furnace producing per ton of hot metal) is about 155 Kg/t, which adopts bell-less roof charging of the parallel tank type. The structure of the roof charging equipment is shown in Figure 3, the parameters and simulation conditions of the charging equipment are shown in Table 6, and the parameters in the table are consistent with the 1750 m<sup>3</sup> BF.

Because of the inherent charging method of the bell-less roof charging equipment, the material flow is biased downward from the center throat to the right wall when the left material tank is discharged, and the right material tank is biased downward to the left wall, which easily causes the segregation of the furnace material at the throat. According to the field measurement, there is segregation of the distribution in the 1750 m<sup>3</sup> BF. To improve the accuracy of the simulation, it is necessary to optimize the model in the simulation stage. The specific model is shown in Figure 4a. The furnace charge generation plane is located below the central throat with the same size as the radius of the central throat, the coke pellets are generated at the red plane (right half part), and the ore pellets are generated at the blue plane (left half part). Figure 4b shows the charging system, showing the whole process of the charge from pellet plant generation to fall to the charge plane. The ore pellets in the figure are classified by color according to their speed: red indicates the fastest speed of the pellets, green indicates moderate speed of the pellets, and blue indicates very slow speed of the pellets or remaining stationary.

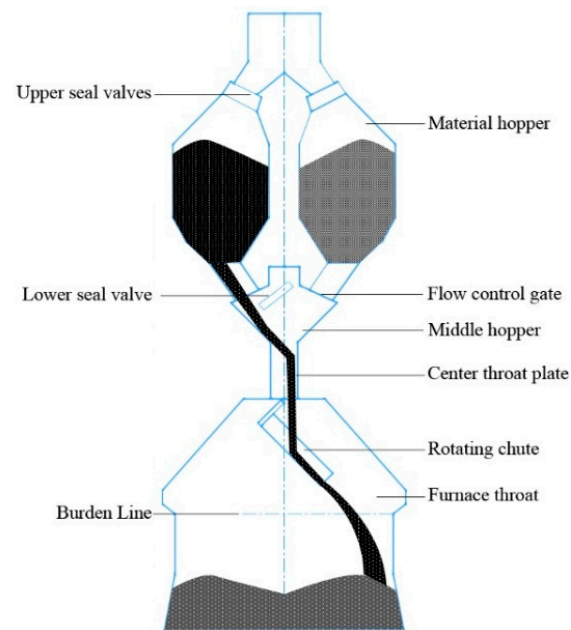


**Figure 3.** Schematic diagram of the parallel-hopper bell-less top.

**Table 6.** Geometric model parameters of charging equipment.

Parameters	Value	Unit
Radius of furnace throat	3450	mm
Chute length	3500	mm
Internal radius of chute	420	mm
Tilting distance of chute	850	mm
Radius of central throat plate	375	mm
Rotation speed of chute	48	$\text{deg}\cdot\text{s}^{-1}$
Tilting speed of chute	10	$\text{deg}\cdot\text{s}^{-1}$
Falling speed of material surface	2	$\text{mm}\cdot\text{s}^{-1}$

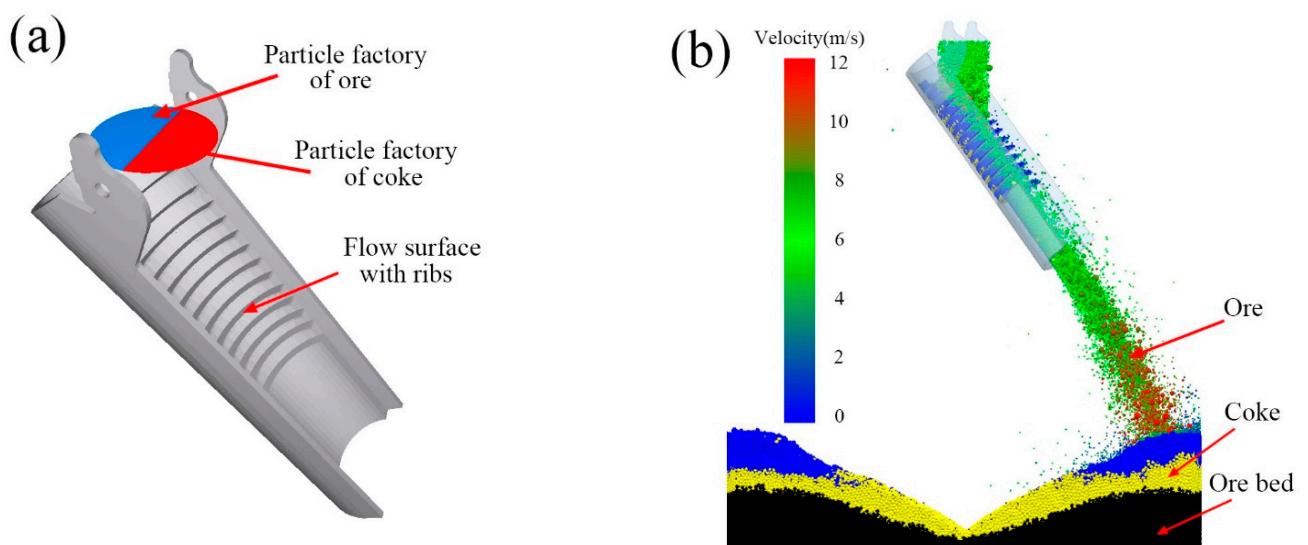


**Figure 4.** Process of particles from generation to falling to the burden surface: (a) burden generation model; (b) charging system.

The restoration coefficient and friction factor between different material particles were discussed above. In this section, several parameter verification experiments are conducted based on Table 5 and the measured data. The final contact parameters are determined as shown in Table 7. In Table 7, the steel refers to the metal chute; since Ore2 is used as the filling of the base material surface (ore bed), the shape of the base burden surface is kept constant throughout the simulation, so the friction factor between Ore2 and Ore2 is not considered.

**Table 7.** Contact parameters between different materials.

Interaction	Restitution Coefficient	Static Friction	Rolling Friction
Coke1–Coke1	0.2	0.13	0.07
Coke1–Coke2	0.2	0.2	0.3
Coke2–Coke2	0.2	0.2	0.3
Coke1–Ore1	0.2	0.3	0.3
Coke2–Ore1	0.2	0.6	0.6
Ore1–Ore1	0.6	0.5	0.1
Coke1–Ore2	0.2	0.3	0.3
Coke2–Ore2	0.2	0.6	0.6
Coke1–Steel	0.4	0.5	0.12
Coke2–Steel	0.4	0.5	0.12
Ore1–Steel	0.4	0.5	0.06

### 3. Results and Discussion

#### 3.1. Model Validation

After determining the contact parameters between materials, the accuracy of the results of the distribution model was verified. Figure 5 shows the measured burden surface shape in the blast furnace and the burden surface shape simulated by the discrete element method. The burden matrix used is C: 38.5° 36.5° 34.5° 32.5° 30.5° 22.5° (222224, the number represents the number of turns of the chute rotation at each angle.), O: 38.5° 36.5° 34.5° 32.5° 30.5° (33321), the ore batch weight is 48 t, the coke batch weight is 9.345 t, and the burden line depth is 1.5 m. From Figure 5, it can be seen that the simulation results of the burden model are close to the measured results in the blast furnace, which confirms the high accuracy of the preset DEM burden model. This experiment is taken as the basic experiment of this paper, and subsequent experiments will be developed on the basis of this experiment to adjust the burden line depth, the batch weight of coke and ore, and the angle of each gear in the burden matrix.

To obtain a more accurate picture of the change pattern of the ore-free zone, it is necessary to quantify it and to count the particle information in the central area of the furnace throat when performing data analysis. The shape of the ore-free zone and the distribution of the furnace charge in the area were calculated. The sampling area is shown in Figure 6. The cylinder in the figure is located in the center of the furnace throat, with a diameter of 2000 mm and a height of 1500 mm, which is the sampling area for analyzing the distribution of the charge in the ore-free zone; the rectangular body in the figure is the sampling area for analyzing the shape of the ore-free zone, with a length of 7000 mm, a width of 400 mm, and a height of 2000 mm.

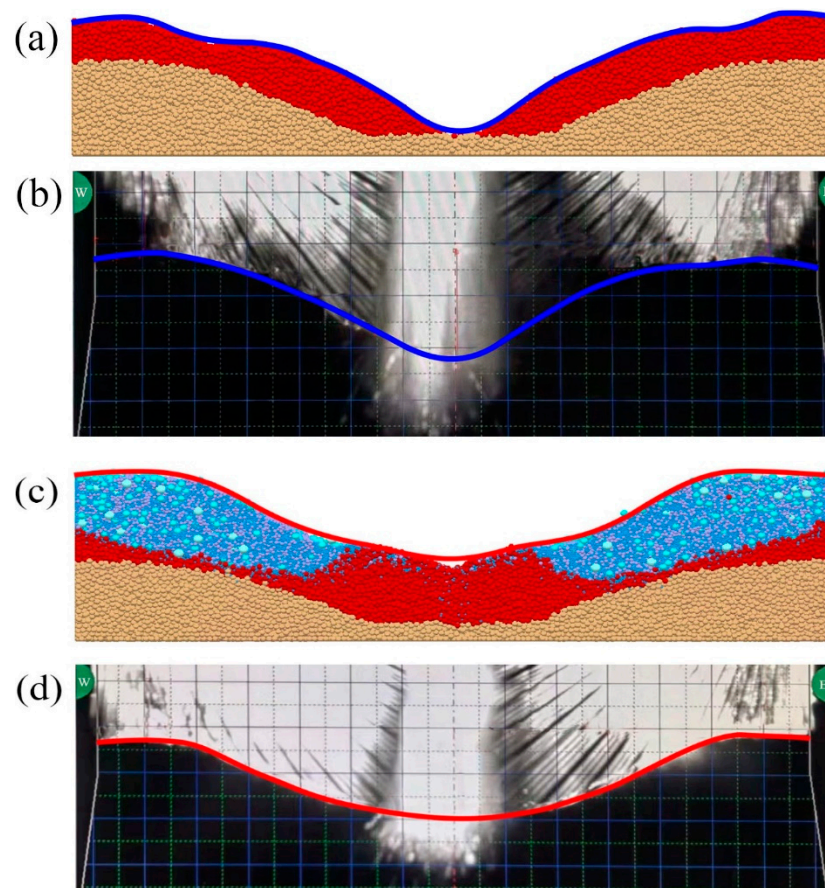


**Figure 5.** Coke burden surface and ore burden surface under base conditions: (a) coke simulated burden surface; (b) coke measured burden surface; (c) ore simulated burden surface; (d) ore measured burden surface.

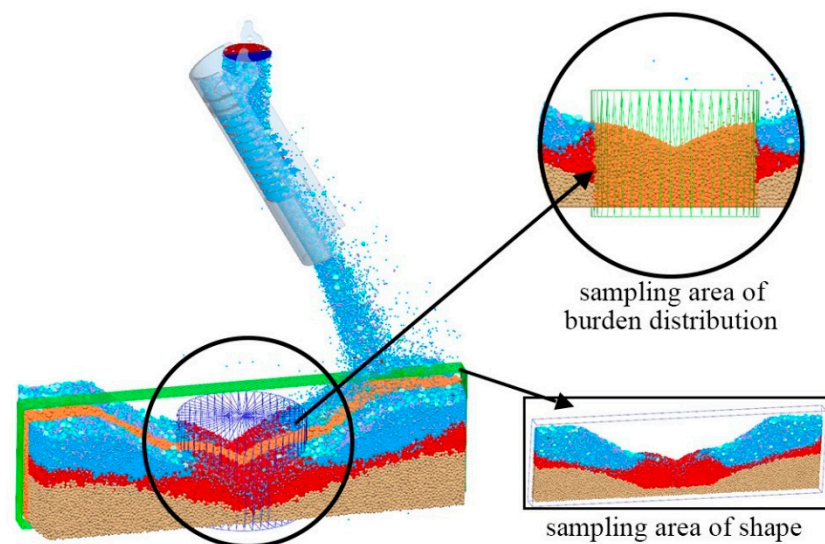


**Figure 6.** The sampling area diagram of data analysis.

### 3.2. Effect of Burden Line Depth on the Formation of Ore-Free Zones

The charging process was simulated with material line depths of 1.2 m, 1.5 m, and 1.8 m, and the influence of the burden line depth on the formation of the ore-free zone was explored by analyzing the burden surface in the sampling area. The corresponding ore-free zone shape

is shown in Figure 7, and the width and thickness of the ore-free zone under different burden line depths are shown in Table 8.

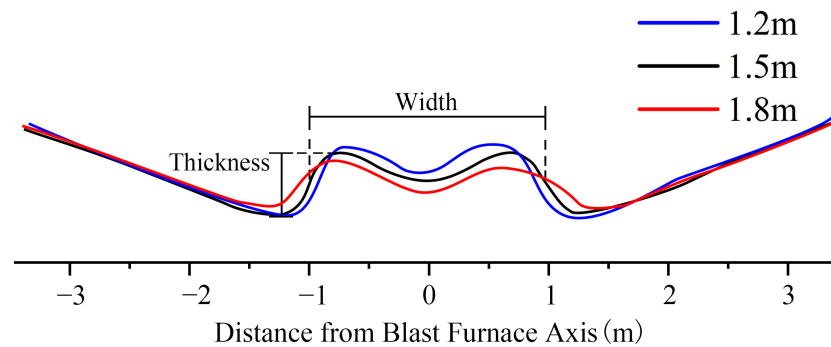


**Figure 7.** Shape of the burden surface of the ore-free zone at different burden line depths.

**Table 8.** Width and thickness of the ore-free zone at different burden line depths.

Burden Line (m)	Width (m)	Thickness (m)
1.2	1.79	0.63
1.5	1.93	0.52
1.8	2.06	0.43

The simulation results show that with the depth of the burden line increasing, the width of the upper part of the ore-free zone increases, and the thickness decreases. This means that with the depth of the burden line increasing, the pushing effect of the ore on the coke becomes weaker because the fall point of the charge moves toward the furnace wall and the ore pushes more coke, which also leads to a decrease in the total mass of ore and coke in the ore-free zone. To verify this idea, the burden distribution within the sampling area was counted, and the analysis results are shown in Figure 8, where ORE-A, ORE-B, ORE-C, and ORE-D refer to ore particles with particle sizes of 20 mm, 34 mm, 64 mm, and 90 mm, respectively, and COKE refers to coke particles with a particle size of 50 mm. From the figure, it can be seen that the total mass of coke particles and ore particles in the sampling area decreases to different degrees with the increase in the depth of the burden line. The calculation method of the mass is shown as follows, and takes the particle size of 34 mm as an example:

$$M = S * m \quad (5)$$

Among them,  $M$  represents the total mass of 34 mm particles in the sampling area;  $S$  represents the total quantity of 34 mm particles in the sampling area; and  $m$  represents the mass of a single 34 mm particle.

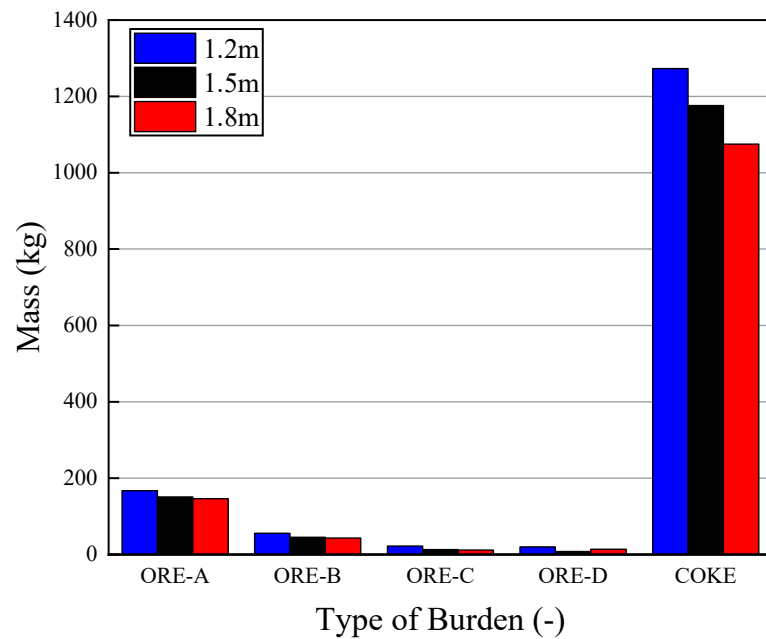


**Figure 8.** Distribution of burden in sampling area under different burden line depths.

The ore–coke ratio curve of the burden surface under different burden line depths is analyzed. The ore–coke ratio curve refers to the ratio of ore quality to coke quality in the area. The sampling area is shown in Figure 9. The dotted rectangle is the sampling area with a width of 100 mm. It moves from the center of the furnace throat (0 mm) to the left and right sides of the furnace wall (−3450 mm and 3450 mm), respectively. Sampling was taken every 100 mm, and a total of 69 sampling areas were taken. The ratio of ore mass to coke mass in each zone was counted, and the results are shown in Figure 10, where the horizontal coordinate is the distance from the center of the furnace throat and the vertical coordinate is the ratio of ore to coke mass in the sampling zone. It can be seen from the figure that as the depth of the burden line increases, the ore–coke ratio near the ore-free zone near the center of the furnace throat decreases and the ore–coke ratio near the furnace wall increases, which indicates that the permeability of the central area is enhanced and the permeability near the furnace wall is weakened for two reasons: first, the mass of coke and ore in the central part of the furnace throat decreases, and second, the cross-sectional area of the ore-free zone is increased. In summary, changing the depth of the burden line causes the thickness of the ore-free zone to decrease, the width to increase, and the area with higher permeability to be enlarged and more favorable to the development of the central airflow.

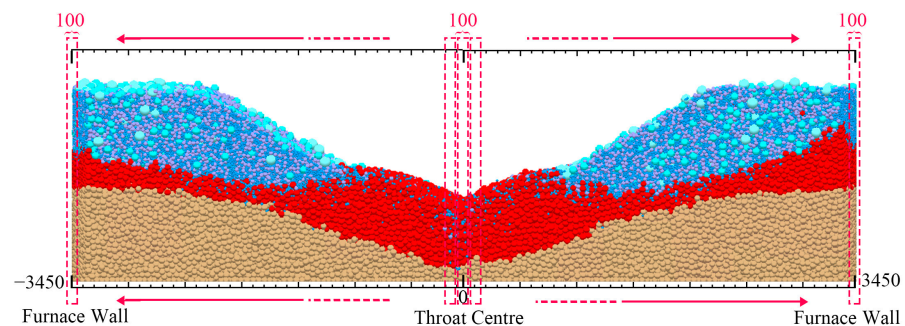


**Figure 9.** Schematic diagram of the delineated sampling area.

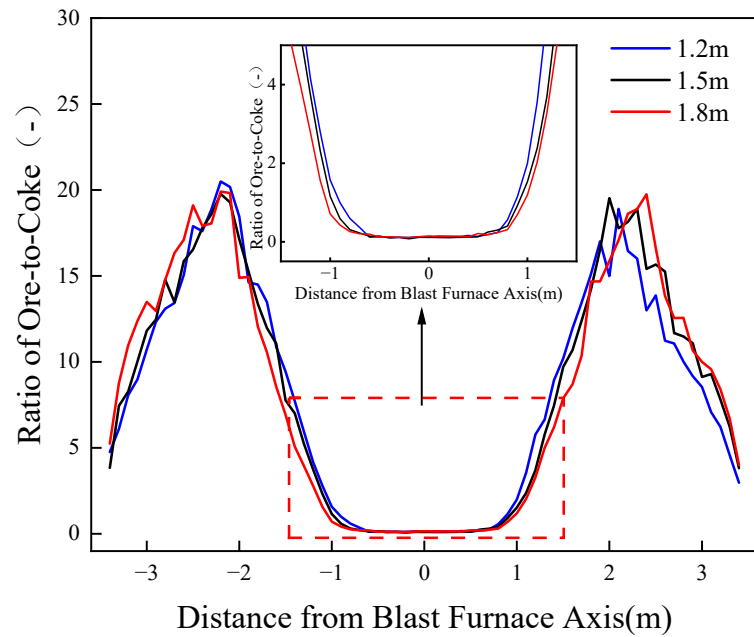


Figure 10. Effect of different burden line depths on the ore-to-coke ratio within the ore-free zone.

3.3. Effect of Burden Batch Weight on the Formation of Ore-Free Zones

The initial batch weight of coke in the basic experiment is 9.345 t, and the batch weight of ore is 48 t. To investigate the effect of the burden batch weight on the formation of the ore-free zone, two sets of comparison experiments were conducted: the first set of experiments is changing the batch weight of ore only, and the second set of experiments is changing the batch weight of coke and ore at the same time.

In the first group of experiments, only the batch weight of ore is changed, the amount of increase or decrease is 1/8 (6 t) of the ore batch weight in the base experiment, and the coke batch weight remains 9.345 t. The shape of the ore-free zone obtained is shown in Figure 11, and the width and thickness of the ore-free zone under different ore batch weights are shown in Table 9.

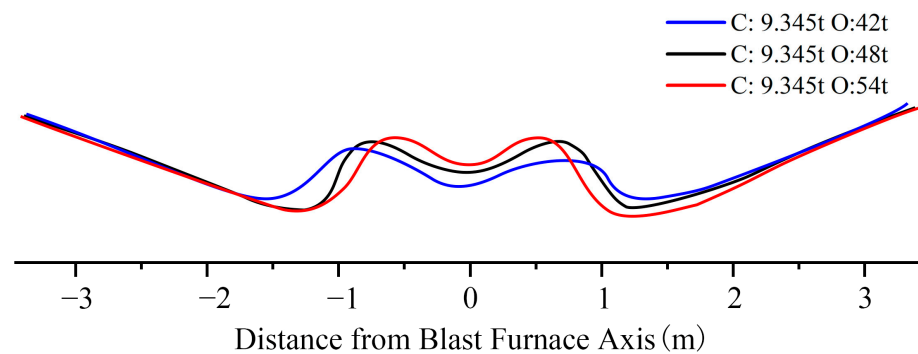
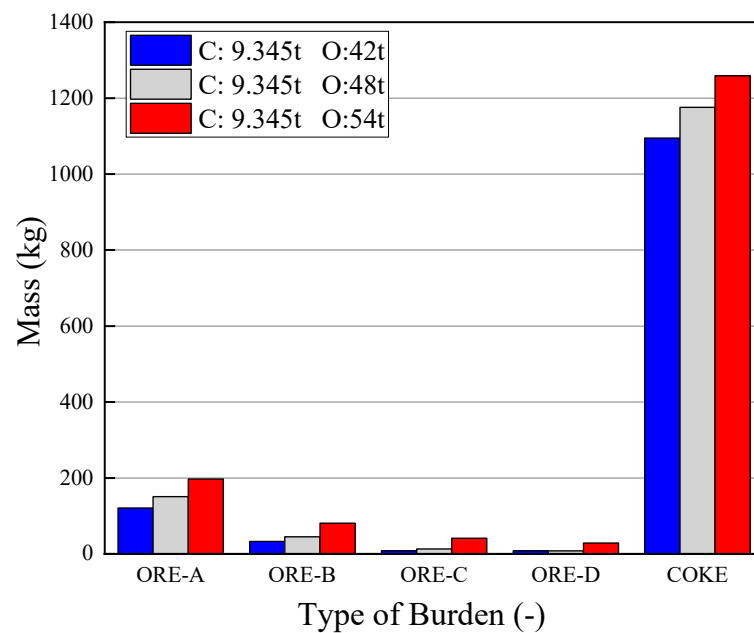


Figure 11. Shape of the ore-free zone with different ore batch weights.

Table 9. Width and thickness of the ore-free zone under different ore batch weights.

Batch Weight (t)	Width (m)	Thickness (m)
C:9.345; O:42	2.23	0.39
C:9.345; O:48	1.93	0.52
C:9.345; O:54	1.71	0.62

The simulation results show that the thickness of the ore-free zone decreases and the width increases when the ore batch weight is reduced, while the thickness of the ore-free zone increases and the width decreases when the ore batch weight is increased. The reason is that with ore batch weight increasing, the ore pushes onto the coke tighter due to the increase in ore distribution, which has a greater impact on the thickness and width of the ore-free zone, while the location of the drop point and the coke batch weight remain unchanged [24]. Figure 12 shows the mass distribution of the charge in the sampling zone in the center of the throat, and the mass of both coke and ore in the sampling zone increases with the ore batch weight increase. The increase in coke mass is due to the increase in ore pushing, which concentrates more coke in the central area, and the increase in ore mass is due to the increase in ore batch weight, which in turn rolls more ore down to the central area; this result also shows that the DEM-based charging simulation can achieve the characterization of the interparticle interaction relationship.



**Figure 12.** Burden distribution in the sampling area under different ore batch weights.

In the second group of experiments, the batch weight of coke and ore increase or decrease by 1/8 of the basic experimental amount at the same time. The shapes of the ore-free zone under three different batch weights are shown in Figure 13, and the width and thickness of each shape are shown in Table 10.

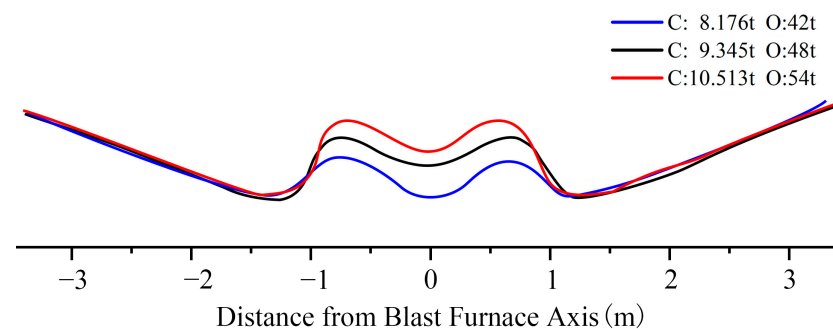


**Figure 13.** Shape of the ore-free zone with different coke and ore batch weights.

**Table 10.** Width and thickness of the ore-free zone under different coke and ore batch weights.

Batch Weight (t)	Width (m)	Thickness (m)
C:8.176; O:42	1.87	0.37
C:9.345; O:48	1.93	0.52
C:10.513; O:54	1.89	0.66

The simulation results show that the thickness of the ore-free zone gradually increases with the increase in the batch weight of the charge, and the change in the width is smaller. The reason is that more coke is pushed onto the ore-free zone by the ore, and since the batch weight of both coke and ore is increased, the pushing effect of coke by the ore hardly changes, while the ore particles that roll down into the central area also increase. Figure 14 shows the mass distribution of the charge within the sampling area in the center of the furnace throat. As the batch weight of the charge increases, there is a significant increase in the mass of coke within the sampling area, and there is also an increase in the mass of ore, but the increase is small, especially when the increase in large particles of ore is very weak.

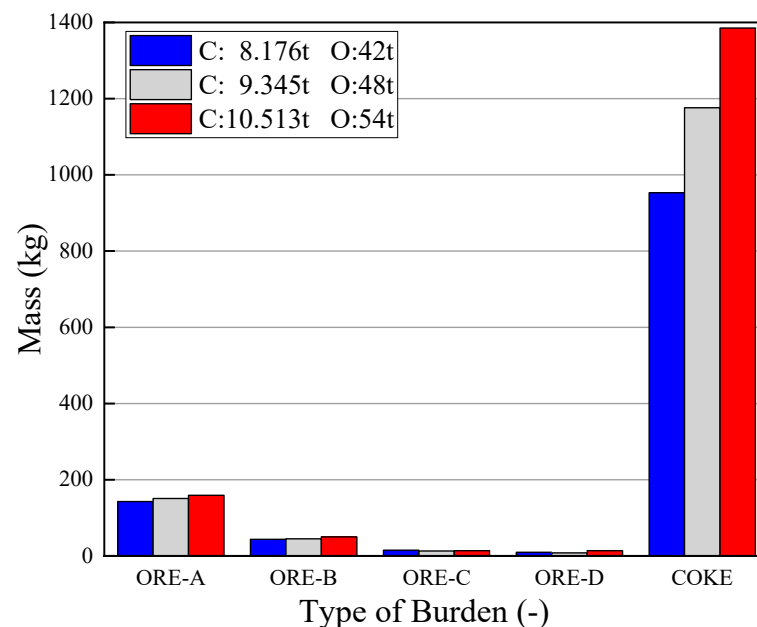
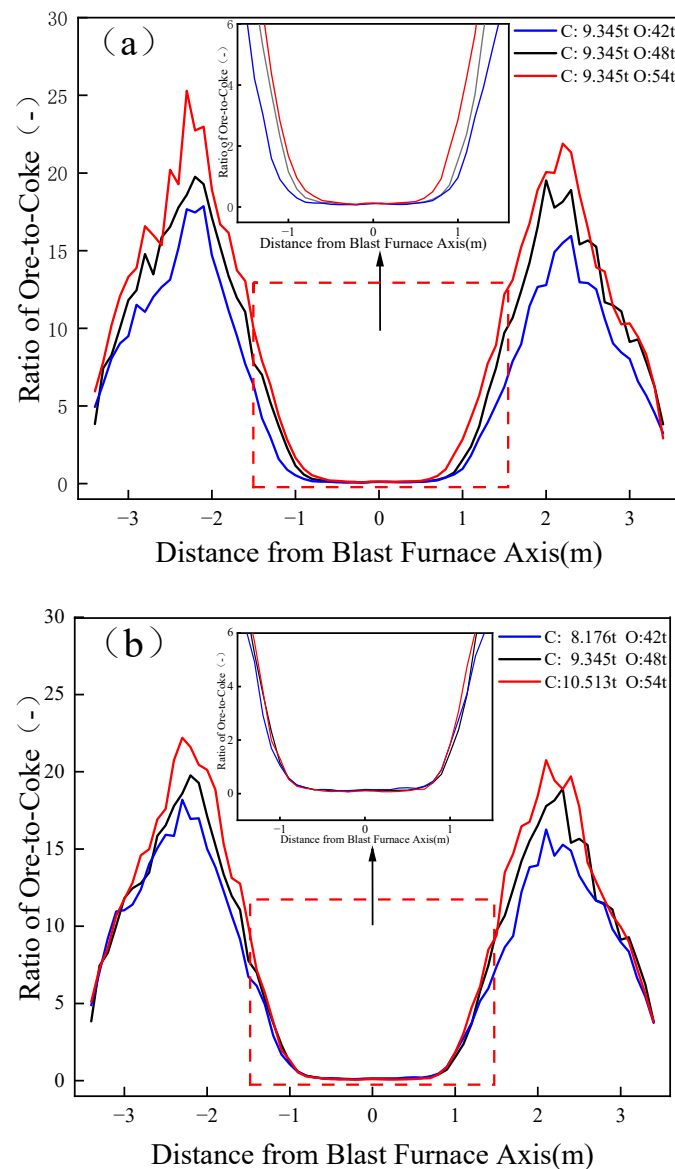
**Figure 14.** Burden distribution in the sampling area under different ore and coke batch weights.

Figure 15 shows the curves of the ore–coke ratio of the two groups of experiments. In the case of only changing the ore batch weight, with the ore batch weight increased, the ore–coke ratio near the ore-free zone increased, resulting in a decrease in the area with high permeability in the center of the blast furnace, and the permeability deteriorated. The increase in the ore–coke ratio near the furnace wall is due to the increase in the ore quality, which also inhibits the development of the airflow. In the case of changing both coke and ore batch weights, with the increase in both batch weights, the ore–coke ratio near the center area and the edge of the furnace wall remains basically unchanged, but the ore–coke ratio in the middle area between the center of throat and the furnace wall increases significantly, thus indirectly promoting the development of gas flow at the edge and the center.



**Figure 15.** Effect of the charge batch weight on the ore-coke ratio within the ore-free zone: (a) change in ore batch weight only; (b) change in coke and ore batch weight at the same time.

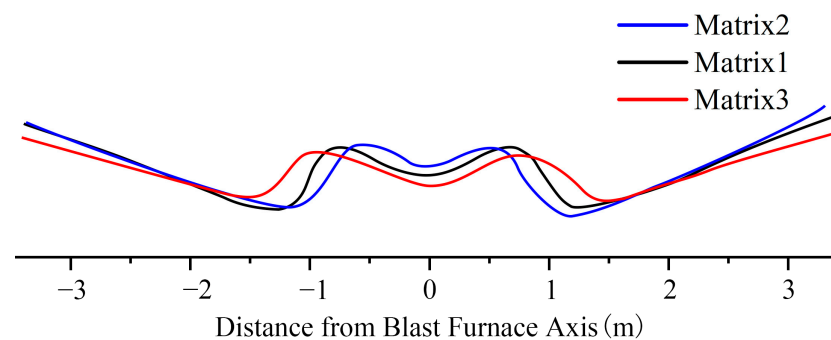
### 3.4. Influence of the Distribution Angle on the Formation of Ore-Free Zones

To investigate the effect of the distribution angle on the formation of the ore-free zone, five burden matrixes are set up in this section, as shown in Table 11. The number of circles in each matrix is fixed: for each coke slot from high to low is 2, 2, 2, 2, 2, 2, and 4, and for each ore slot from high to low is 3, 3, 3, 2, and 1. Therefore, only the angles are shown in the table, where Matrix1 is the burden matrix for the basic experiment. In this section, two sets of experiments are conducted. The first set of experiments is keeping the distribution angle of coke unchanged and changing only the angle of ore in the matrix, corresponding to Matrix2 and Matrix3; the second set of experiments is changing the angle of coke and ore in the matrix at the same time, corresponding to Matrix4 and Matrix5.

**Table 11.** Burden matrix design scheme.

Type	Number	burden	Charging Angle					
Fundamental experiment	Matrix 1	C	38.5	36.5	34.5	32.5	30.5	22.5
		O	38.5	36.5	34.5	32.5	30.5	-
First group of experiments	Matrix 2	C	38.5	36.5	34.5	32.5	30.5	22.5
		O	36.5	34.5	32.5	30.5	28.5	-
	Matrix 3	C	38.5	36.5	34.5	32.5	30.5	22.5
		O	40.5	38.5	36.5	34.5	32.5	-
Second group of experiments	Matrix 4	C	36.5	34.5	32.5	30.5	22.5	20.5
		O	36.5	34.5	32.5	30.5	28.5	-
	Matrix 5	C	40.5	38.5	36.5	34.5	32.5	24.5
		O	40.5	38.5	36.5	34.5	32.5	-

In the first set of experiments, only the angle of the ore in the burden matrix is changed. The ore-free zone shapes under three different matrices are shown in Figure 16, and the width and thickness of each shape are shown in Table 12.

**Figure 16.** Effect of changing only the angle of the ore in the matrix on the shape of the ore-free zone.**Table 12.** Width and thickness of the ore-free zone when changing only the angle of the ore in the matrix.

Matrix	Width (m)	Thickness (m)
Matrix 2	1.64	0.71
Matrix 1	1.93	0.52
Matrix 3	2.24	0.44

The simulation results show that the width of the ore-free zone gradually increases and the thickness gradually decreases with the ore angle increasing in the burden matrix, and the increase in width is larger and the decrease in thickness is smaller. The reason is that with the increase in ore angle, the ore landing point position gradually moves toward the furnace wall, and thus, the pushing effect of the ore on the coke is weakened, thus forming a wider but narrower ore-free zone. Figure 17 shows the mass distribution of the charge within the sampling zone at the center of the furnace throat. From the figure, it can be seen that the mass of ore and coke within the sampling zone gradually decreases as the angle of the ore increases, which can also reflect that the amount of coke pushed into the center of the furnace throat by the ore decreases due to the weakening of the pushing effect of the ore on the coke.

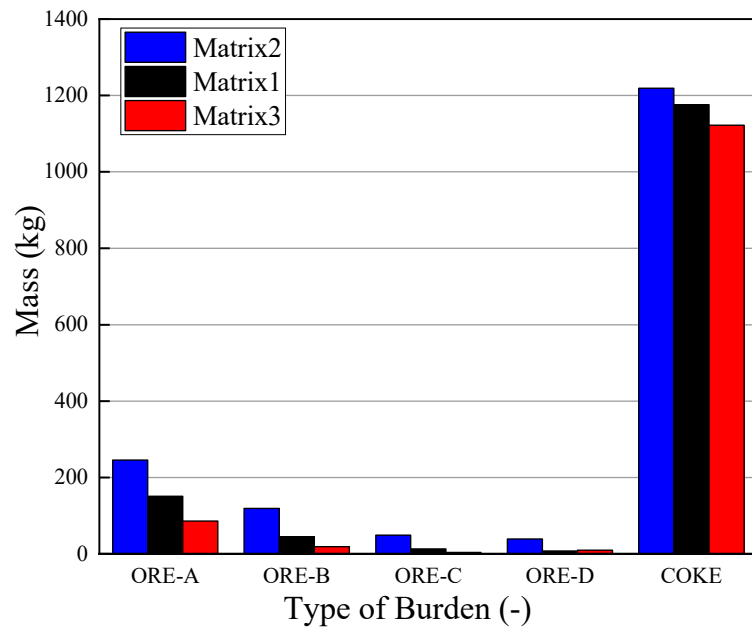


**Figure 17.** Distribution of charge within the sampling zone in different fabric matrices under the condition that only the angle of the ore in the matrix is changed.

In the second set of experiments, the angle between the coke and the ore in the matrix is changed simultaneously. The ore-free zone shapes under the three different matrices are shown in Figure 18, and the width and thickness of each shape are shown in Table 13.

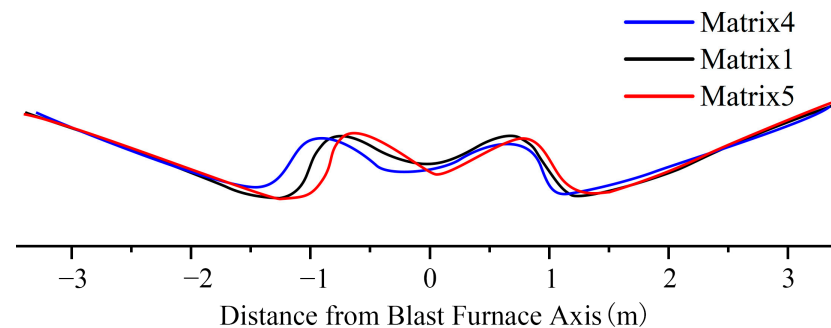


**Figure 18.** Effect of simultaneously changing the coke and ore angles in the matrix on the shape of the ore-free zone.

**Table 13.** Width and thickness of the ore-free zone under the condition of simultaneously varying the coke and ore angle in the matrix.

Matrix	Width (m)	Thickness (m)
Matrix 4	2.17	0.47
Matrix 1	1.93	0.52
Matrix 5	1.87	0.55

From the simulation results, it can be seen that the width of the ore-free zone gradually decreases with the simultaneous increase in the coke and ore angle, and at the same time, compression of the ore-free zone shape to the right occurs. Figure 19 shows the mass distribution of the charge within the sampling zone in the center of the furnace throat. With the increase in coke and ore angle, there is a significant decrease in coke mass and an increase in ore mass in the sampling zone.

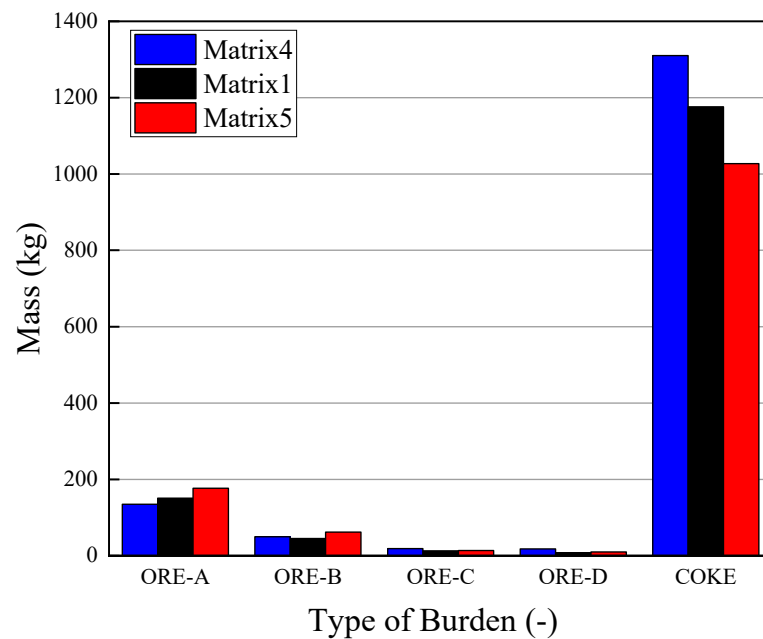


**Figure 19.** Distribution of charge in the sampling area under different burden matrices with simultaneous changes in coke and ore angles in the matrix.

There are several reasons for the above phenomenon: first, when the angle of coke increases, the coke in the center of the furnace throat will decrease, and when the angle of ore increases, the position of the ore drop point will be closer to the furnace wall, and the pushing and squeezing effect of the ore on coke is weakened, resulting in the reduction in the ore-free zone; therefore, with the angle of coke and ore in the matrix gradually increasing, the ore-free zone will gradually decrease. Another thing that needs to be considered is the segregation of the charge. The charging model used in this paper is introduced in Section 2.3. The model takes into account the segregation of the charge caused by the parallel material tank, as shown in Figure 20. When the chute rotates at different angles, the speed of the burden leaving the chute is different, as shown in Figure 20a. Under the conditions of Matrix4, Matrix1, and Matrix5, when the chute angle is  $90^\circ$  in the circumferential direction, the speed of the ore leaving the chute is 2.83 m/s, 3.13 m/s, and 3.37 m/s, respectively, and the difference among the three speeds is large. When the chute angle is  $270^\circ$  in the circumferential direction, the speed of ore leaving the chute is 2.35 m/s, 2.42 m/s, and 2.51 m/s, respectively, and the difference among the three speeds is small.

Figure 21 shows the ore-to-coke ratio curves in the two groups of experiments. In the case of only changing the ore angle in the matrix, with the increase in the angle, the ratio of ore to coke near the ore-free zone decreases, the width of the ore-free zone increases, and the thickness decreases, which promotes the development of the central airflow. The increase in the ore-to-coke ratio near the furnace wall is because the ore falling point moves toward the furnace wall and the ore quality increases, thus inhibiting the development of the edge airflow. In the case of changing the angle of coke and ore in the matrix at the same time, with the increase in the angle of the two, the ore-to-coke ratio on the left side near the ore-free zone in the central area increases, the width of the ore-free zone decreases, and the thickness is basically unchanged, which leads to the reduction in the area with better permeability and inhibits the development of airflow. At the same time, only the central region shows an obvious segregation phenomenon, and the ore-to-coke ratio in the edge region shows the opposite situation in the left and right regions. This shows that when changing the ore and coke cloth angle at the same time, it is necessary to pay attention to the segregation phenomenon of airflow distribution.

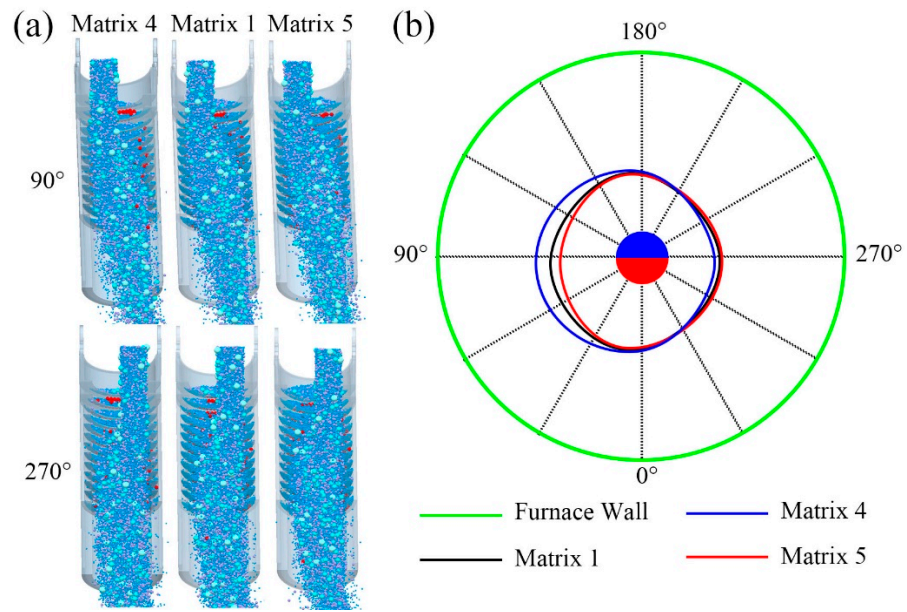


**Figure 20.** Segregation phenomenon under different cloth matrix by changing the angle of coke and ore in the matrix: (a) movement of the charge in the chute with different burden matrices; (b) contours of the edge of the ore-free zone with different burden matrices.

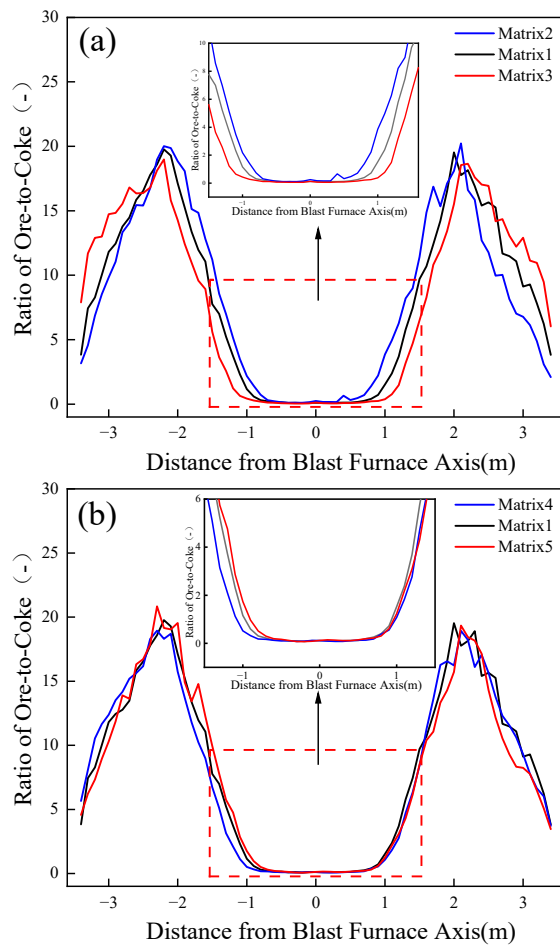


**Figure 21.** Effect of the distribution angle on the ore-to-coke ratio within the ore-free zone: (a) only changing the ore angle; (b) changing both the coke and ore angles.

#### 4. Conclusions

The formation of an ore-free zone in the center of the furnace throat is an important means to improve the permeability of the center of the blast furnace. In this paper, the formation of an ore-free zone in the upper part of the blast furnace is simulated by using the discrete element method based on the 1:1 three-dimensional model of the blast furnace. The effects of burden line depth, charge batch weight, and distribution angle on the formation of the ore-free zone were studied, and the results are as follows:

- (1) With the depth of the burden line increasing, the width of the ore-free zone increases, the thickness decreases, and the ore-to-coke ratio decreases, because the cross-sectional area of the ore-free zone increases and the central airflow is developed. Therefore, in actual production, increasing the depth of the material line can be used to further develop the central airflow and suppress the marginal airflow.
- (2) Only changing the ore batch weight will affect the thickness and width of the ore-free zone and have a greater impact on the permeability of the ore-free zone. The greater the ore batch weight, the greater the thickness of the ore-free zone, the smaller the width, and the worse the permeability. Changing the batch weight of coke and ore at the same time mainly affects the thickness of the ore-free zone. The larger the batch weight of coke and ore, the greater the thickness of the ore-free zone, which has less of an effect on the permeability of the ore-free zone compared with changing only the batch weight of ore, so in actual production, from the perspective of optimizing the permeability of the charge, the batch weight of ore and coke should be adjusted at the same time as much as possible.
- (3) In the case of changing only the angle of the ore in the matrix, the ore-to-coke ratio near the ore-free zone decreases as the angle increases, mainly because the width of the ore-free zone increases and the thickness decreases, which promotes the development of central airflow, while the ore-to-coke ratio near the furnace wall increases because the ore drop point moves toward the furnace wall and the ore mass becomes greater, thus inhibiting the development of airflow. In the case of changing the angle of coke and ore at the same time, with the gradual increase in the angle of the two, the ore-free zone will gradually compress in the direction of smaller segregation of the burden, and the ratio of ore to coke in the central area will increase. The reason is that the width of the ore-free zone is reduced and the thickness is basically unchanged, resulting in a decrease in the area with better permeability and inhibiting the development of the airflow. When there is segregation in the blast furnace, the gas flow at the center of the furnace throat can be adjusted by changing the distribution angle of coke and ore.
- (4) Through the research of this paper, it is further concluded that the influence on the central ore-free zone under different burden systems should consider the behavior of the extrusion between the ore-coke in addition to the location of the furnace charge drop point, and special attention should also be paid to the segregation phenomenon of the charging at the top of the bell-less blast furnace of the parallel tank type to improve the accuracy of the control of the charging.

**Author Contributions:** Conceptualization, B.Y. and C.L.; methodology, B.Y. and H.X.; software, H.X.; validation, H.X.; formal analysis, H.X. and B.Y.; investigation, C.L.; resources, H.G. and C.L.; data curation, H.X.; writing—original draft preparation, H.X.; writing—review and editing, H.X. and B.Y. and Y.W.; visualization, H.X.; supervision, B.Y. and Y.W. and H.G.; project administration, B.Y.; funding acquisition, H.G. All authors have read and agreed to the published version of the manuscript.

**Funding:** This work is sponsored by the National Natural Science Foundation of China (NO. 52074185, NO. 51774209) and the Suzhou Science and Technology Plan Project (NO. SYG202127).

**Data Availability Statement:** The datasets used and/or analyzed during the current study are available from the corresponding author on reasonable request.

**Conflicts of Interest:** We declare that none of the authors have any financial or scientific conflicts of interest with regard to the research described in this manuscript.

## References

1. Wang, Z.; Zhang, H.; Li, H.; Teng, Z. Evolution and optimization of charging sequence for No.1 BF in Shougang Jingtang. *IRONMAKING* **2017**, *36*, 5–9.
2. Li, L.; Chen, J.; Li, X.; Wang, Z.; Li, B. Adjustment and Optimization of the Masteel's No.4 BF Charging System. *IRONMAKING* **2019**, *38*, 19–23.
3. Zhao, G.; Cheng, S.; Xu, W.; Li, C. Mechanism of burden distribution in central coke charging process and exploration on charging pattern in blast furnace. *Iron Steel* **2016**, *51*, 10–18.
4. Wu, H.; Ling, M. Study on Burden Distribution Pattern Regulation in Masteel's 4000 m<sup>3</sup> BF. *IRONMAKING* **2016**, *35*, 11–14.
5. Xia, X.; Zhou, L.; Ma, H.; Zhao, Y. Effect of particle shape model on DEM simulation of charging process in blast furnace. *J. Iron Steel Res.* **2021**, *33*, 1228–1236.
6. Teng, Z.; Cheng, S.; Zhao, G. Influence of Central Coke Charging on the Gas Distribution and Utilization for a Blast Furnace. *J. Iron Steel Res.* **2014**, *26*, 9–14.
7. Fabian, P.; Alexander, B.; Dieter, S. Effect of pulverized coal residues on the blast furnace streaming conditions. *Ironmak. Steelmak.* **2022**, *49*, 898–904.
8. Li, M.; Wei, H.; Ge, Y.; Xiao, G.; Yu, Y. A Mathematical Model Combined with Radar Data for Bell-Less Charging of a Blast Furnace. *Processes* **2020**, *8*, 239. [[CrossRef](#)]
9. Teng, Z.; Cheng, S.; Du, P.; Guo, X. Mathematical model of burden distribution for the bell-less top of a blast furnace. *Int. J. Miner. Metall. Mater.* **2013**, *20*, 620–626. [[CrossRef](#)]
10. Zhao, G.; Cheng, S.; Xu, W.; Li, C. Comprehensive Mathematical Model for Particle Flow and Circumferential Burden Distribution in Charging Process of Bell-less Top Blast Furnace with Parallel Hoppers. *ISIJ Int.* **2015**, *55*, 2566–2575. [[CrossRef](#)]
11. Wang, L.; Zhang, B.; Zhang, Y.; Cui, G.; Shi, L. Mathematical model of charging shape in bell-less blast furnace burden distribution. *J. Iron Steel Res.* **2018**, *30*, 696–702.
12. Mitra, T.; Saxén, H. Simulation of Burden Distribution and Charging in an Ironmaking Blast Furnace. *IFAC PapersOnLine* **2015**, *48*, 183–188. [[CrossRef](#)]
13. Han, W.; Ding, W.; Li, Y.; Nie, H.; Saxén, H.; Long, H.; Yu, Y. Porosity distribution of moving burden layers in the blast furnace throat. *Granular Matter.* **2021**, *23*, 10.
14. Liu, J.; Huang, M.; Sun, J.; Di, Z.; Ren, H. Study on material flow trajectory with DEM for bell-less top charging of blast furnace. *J. Iron Steel Res.* **2020**, *33*, 1253–1259.
15. Ma, H.; Wang, Z.; Dai, J.; Yuan, J.; Li, X.; Wang, Y. Segregation of material flow under different chute shapes. *Iron Steel.* **2020**, *55*, 23–28.
16. Mio, H.; Narita, Y.; Nakano, K.; Nomura, S. Validation of the Burden Distribution of the 1/3-Scale of a Blast Furnace Simulated by the Discrete Element Method. *Processes* **2019**, *8*, 6. [[CrossRef](#)]
17. Liu, H.; Ning, X.; Wang, Z.; Zhang, J.; Li, R.; Lan, D. Simulation of gas flow velocity and pressure field under central coking system in blast furnace. *China Metallurgy* **2022**, *32*, 46–51.
18. Chakrabarty, A.; Basu, S.; Nag, S.; Ghosh, U.; Patra, M. Model Study of Centre Coke Charging in Blast Furnace through DEM Simulations. *ISIJ Int.* **2021**, *61*, 782–791. [[CrossRef](#)]
19. Xu, W.; Cheng, S.; Niu, Q.; Zhao, G. Effect of the Main Feeding Belt Position on Burden Distribution during the Charging Process of Bell-less Top Blast Furnace with Two Parallel Hoppers. *ISIJ Int.* **2017**, *57*, 1173–1180. [[CrossRef](#)]
20. Narita, Y.; Mio, H.; Orimoto, T.; Nomura, S. DEM Analysis of Particle Trajectory in Circumferential Direction at Bell-less Top. *ISIJ Int.* **2017**, *57*, 429–434. [[CrossRef](#)]
21. Satou, S.; Stephan, S.; Oishi, Y.; Kawai, H.; Nogami, H. Permeation and Blockage of Fine Particles Transported by Updraft through a Packed Bed. *ISIJ Int.* **2020**, *60*, 1551–1559. [[CrossRef](#)]
22. Kou, M.; Wu, S.; Zhou, H.; Yu, Y.; Gu, K. Measurements and application of burden coefficients for DEM simulation in blast furnace. *Iron Steel.* **2018**, *53*, 30–36.
23. Yu, Y.; Saxén, H. Effect of DEM Parameters on the Simulated Inter-particle Percolation of Pellets into Coke during Burden Descent in the Blast Furnace. *ISIJ Int.* **2012**, *52*, 788–796. [[CrossRef](#)]
24. Jimenez, J.; Mochón, J.; Formoso, A. Burden Distribution Analysis by Digital Image Processing in a Scale Model of a Blast Furnace Shaft. *ISIJ Int.* **2000**, *40*, 114–120. [[CrossRef](#)]

**Disclaimer/Publisher's Note:** The statements, opinions and data contained in all publications are solely those of the individual author(s) and contributor(s) and not of MDPI and/or the editor(s). MDPI and/or the editor(s) disclaim responsibility for any injury to people or property resulting from any ideas, methods, instructions or products referred to in the content.